SMAR 2017 – Fourth Conference on Smart Monitoring,
Assessment and Rehabilitation of Civil Structures

SMAR 2017

Structural health monitoring of airfield pavements using distributed fiber-optics sensing

Carlo Rabaiotti[1], Dominik Hauswirth[1], Frank Fischli[1], Massimo Facchini[2], and Alexander Puzrin[1]

[1] ETH Zurich, Zurich, Switzerland
[2] Brugg AG, Brugg, Switzerland

Airfield pavements are subjected to considerable loading and their condition should be steadily monitored for serviceability and safety issues. Additionally, maintenance has to be reduced to a minimum owing to the limited time windows available for repairing. Finding the optimum time of intervention based on the deteriorating conditions of their infrastructure is an important issue for airport authorities. In this paper it is shown how embedded distributed fiber-optic sensors represent a valuable measurement technology to obtain crucial information on the pavement condition.

Different fiber-optic strain sensors have been implemented for this purpose in an asphalt test track at Zurich Airport in order to measure the strains in an airfield pavement induced by the loading of an aircraft. The preliminary assessment of the measurements shows that the cables were able to withstand the harsh condition during construction of the pavement and to measure accurately the strain field in the pavement during operation. Additionally, the measured pavement strain fields also allowed for back-calculation of the pavement material layer stiffness.

1 INTRODUCTION

Structural health monitoring in pavements is usually carried out with non-destructive surface testing, like e.g. Falling Weight Deflectometer (FWD), Benkelman Beam, ETH Delta (Rabaiotti, 2009) or Ground Penetration Radar (GPR) between others or with sensors embedded in the pavement, like accelerometers (Arraigada, 2009) or strain gages.

Sensors embedded in the pavement have a considerable advantage compared to surface testing, since they allow for direct measurements of the strain determining directly and precisely the level of distress in the pavement without inverse analysis. Major disadvantages of this technology are between others, the robustness requirements, since many sensors do not survive installation during pavement construction and the fact that they only give discrete information.

Fiber-optics sensing' technology contributed to development of a new branch of embedded sensors which became adopted in the field of civil engineering and allow overcoming some of these disadvantages. In particular the adoption of distributed fiber-optic sensing technology to measure strain in the pavements is quite promising and has been described by some authors for road pavement applications (e.g. Chapeleau et al., 2014; Wang & Xiang, 2016). Wang & Xiang (2016) studied in particular the influence of strain transfer between the fiber and an asphalt

mastic layer, where the fibers are inserted. This layer is laid out before the next asphalt layers is brought and compacted on top and melted during construction of the pavement.

A crucial aspect in the implementation of distributed fiber-optic sensors in the pavements is to avoid damage of the cables during compaction of the layers and in particular asphalt layers at high temperature, usually in excess of 140 °C. The Brugg Cables company developed ad hoc cables for harsh conditions which were used here for the implementation in asphalt. Their ability to withstand high temperature and to maintain their properties, is investigated in this paper.

2 DESCRIPTION OF THE CABLES

The selected cable designs share common quality and reliability characteristics required by the installation and operation procedures. The cable design and the selected materials have to cope with rough mechanical influences, extreme temperatures, pressure and corrosion by harmful chemicals. All optical losses must be kept as low as possible to avoid degradation of the native instrument's distance range (optical power budget). Installation of fixation elements, optical connections, loops and repair of eventually damaged sensors should be compatible with cable design and field operations.

Two families of fiber-optic cables have been considered and installed in this project: strain sensing cables and temperature sensing cables. The first are aimed to provide a direct measurement of the strain field in a spatially distributed way (i.e. continuously along the cable length). The latter are mainly used to measure the temperature in the vicinity of the strain cables, to provide for a compensation of any thermal effects on the strain measurement during operation. Both strain and temperature precision and localization accuracy depend on the sensor design as well as on the selected measurement technology.

Two types of BRUsens strain sensing cables were selected, tested and installed (BSST-V3 (V3) and BSST-V9 (V9)), as well as one BRUsens temperature sensing cable (BSTE 85°C Metallic (T)), as shown in Figure 1 and 2.

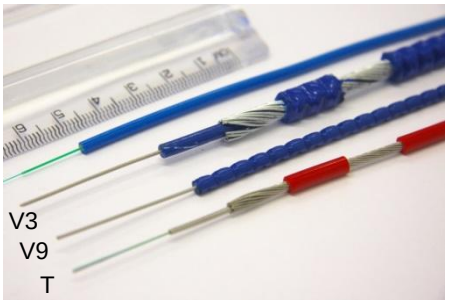

Figure 1: Fiber-optic sensing cables

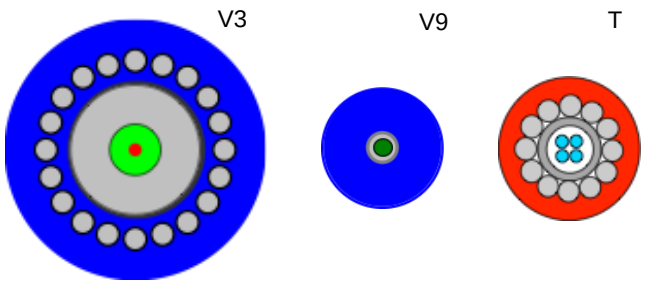

Figure 2: Schematic cross sections the applied cables

BSST-V3 and V9 are flexible, armoured fiber-optic strain sensing cables with central metal tube protecting one tight-buffered optical fiber, structured PA outer sheath, allowing typical measurement strain range up to 1%. The specific benefits provided by these metallic designs are high tensile stiffness (typically around 5000 N/% for the metallic wire armored version V3 and around 560 N/% for V9) and strength, longitudinal and lateral water tightness (even at high hydrostatic pressures), excellent rodent protection, high strain sensitivity, relatively compact

design (7.2 mm or V3 and 3.2 mm outer diameter for V9), good flexibility, abrasion resistant structured halogen-free sheath for better strain transfer in embedded installation, such as in soil, concrete, or asphalt. Among the many available designs of BRUsens Temperature, the BSTE 85°C Metallic (T) version was selected for this application but not used for the purpose of this study. This sensor is a small (3.8 mm outer diameter) armored fiber-optic temperature sensing cable, with stainless steel loose tube (necessary for a potential decoupling the optical fibers from the strain eventually acting on the cable from the environment), stainless steel strength members and PA outer sheath, providing fast thermal response.

Although originally developed for application at temperature up to 80 °C, all cables survived the installation in the asphalt layer, where temperature as high as 140 °C can be reached for several minutes and simultaneously undergo high lateral pressures under the weight of heavy machinery like roller compactors.

3 ADOPTED MEASURING TECHNOLOGY

Distributed fiber-optic sensors allow for continuously measuring strain and temperature changes along a standard optical single mode fiber. Different measurement technologies exist nowadays. In the present project, BOTDA (Brillouin optical time domain analysis, e.g. Horiguchi et al., 1989; Niklès et al., 1997; Niklès, 2007) and SWI (Swept wavelength interferometry, e.g. Froggatt & Moore, 1998; Gifford et al., 2007) were applied. Whereas the former technology is based on stimulated Brillouin scattering, the latter is built on Rayleigh scattering. The present article contains only SWI measurement results, which were obtained by using a commercially available measurement unit. Both quantities, temperature and strain, induce a measurable spectral shift, which can be continuously localized along the fiber. If strain and temperature in a measurement affect the fiber simultaneously, a separation method has to be applied. Various methods exist for this purpose e.g. the simultaneous usage of different cables (loose tube, tight buffered), where the loose tube fiber is isolated from strain or the simultaneous application of different measurement technologies with not equal sensitivities to strain and temperature on a tight buffered cable (e.g. Kishida et al., 2012; Mohamad, 2012).

The Rayleigh scattering based technology (SWI) was adopted as the primary sensing technology in this project. Although the maximum sensor length is limited to around 70m (at the selected instrument performance), the particular measurement unit offers the possibility of measuring with high spatial resolution, which appeared to be crucial for the high spatial strain gradients present in asphalt in this specific project.

4 LABORATORY TESTING

As the direct embedment into asphalt forms a rather harsh environment (temperature, contact pressures), the fiber-optic cables were tested in the laboratory before they were applied in the field. In order to exclude any detrimental effects on the performance (conversion of frequency shift measured to strain) of the cable due to the high temperatures during pavement construction, the strain response of cable BSST-V9 was first measured at different levels in a strain test bed. Afterwards the cable was exposed to different temperatures ranging from room temperature to around 140 °C. Although the cable behaviour (thermal expansion, shrinkage of the cable sheath) was found during the thermal stage of the test to be non-linear and partially irreversible for the highest temperatures, the strain response of the cooled down cable in a subsequent test in the strain test bed did not change noteworthy compared to the initial test. However, the thermal behaviour of the V3 cable requires further investigation.

5 TEST FIELD

The test field has been built in a new pavement for temporary use at Zurich Airport. The pavement layers consist of two asphalt layers (AC 11S and AC B 22 S) and 2 cement treated soil layers (ZMO and ZMU). The thicknesses are shown in Figure 3.

The strain and temperature sensors were embedded in two layers of the pavement (Figure 3). The BSST-V3, BSST-V9 and BSTE sensing cables were installed on the bearing layer in loops of around 150 m each (4 cm depth), accessible for measurements from both sides. Another loop of around 150 m BSST-V3 cable was installed on the foundation layer (13.5 cm depth).

The sensors were first laid out on the substrate layer and positioned correctly. In a second step, the cables were pre-strained and fixed in place. For a better protection in the harsh conditions of the rolling compactor machine, the sensors were then covered manually with finer asphalt, before the overlying layer was built-in. Figure 4 shows selected steps of the installation process.

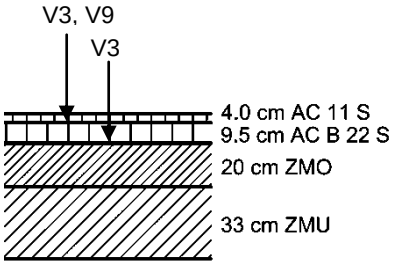

Figure 3: Pavement cross section with position cables. ZMO an ZMU represent the CTB layers

Figure 4: Selected steps of the sensor installation process

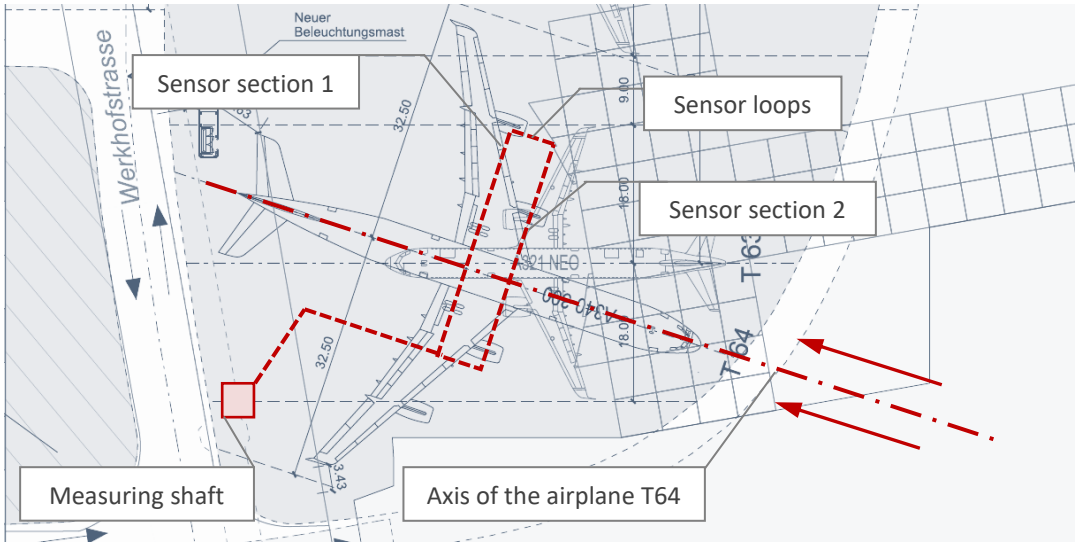

Figure 5: Schematic sketch (plan view) of the installed sensor loops with respect to the axis of the airplane (T64)

The sensor loops were installed perpendicular to the axis T64 of the airplane with the two sensor legs (section 1 & 2) having a distance of 6 m between each other. During the testing, the airplane was pushed backwards along the axis T64 and measurements were taken in different distances to the sensing loops (Figure 6, positions $a_1 – a_4$, having a distance from the main gear axis to the sensor cable section 1 of 10 m to 0 m). A baseline reading was taken before arrival of the airplane (position a_0). The airplane was then stopped during the push-back to take readings in the positions $a_1 – a_4$, where during the foreseen position a_3 the center of the rear tires stands on sensor section 1 ($x = 1$ m) and during the foreseen position a_4 the center of the main gears (but not of any tires) is located above sensor section 1 ($x = 0$ m). Unfortunately the airplane was slightly misplaced during the test, which resulted in an offset of approximately 1.1m on the *y*-axis and a small deviation of the rear main gear axis to the axis of cable section 1 (Figure 6). Hence, during position a_3, the center of the rear tires of the main gear 2 stood approximately directly above cable section 1, but the rear tires of the main gear 1 where slightly displaced from cable section 1.

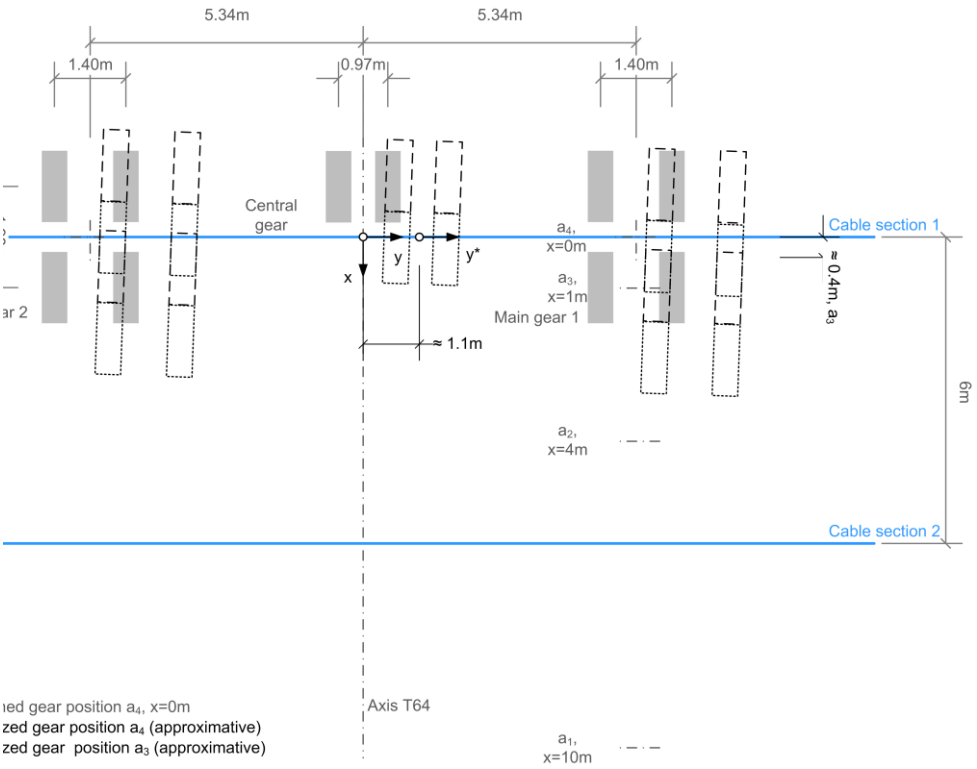

Figure 6: Measuring position of the rear landing gear relative to the sensor loops

6 MEASUREMENT RESULTS

In the following figures, the strains measured along different fiber-optic cables in section 1 are shown for the respective airplane positions according to Figure 6. The strain was measured perpendicular to the airplane axis (along the shifted coordinate *y**) using a commercially available SWI-unit with a spatial strain resolution of 10 mm.

Figure 7 shows the strain distribution along the BSST-V9 cable in a depth of 4 cm just above the AC22 layer. For airplane positions a_1 and a_2, the induced strains are not measurable or for a_2 very small. However, relatively large strains were measured at position a_3, where the center of the rear tires of the main gear 2 is approximately located directly above the cable, whereas the center of the rear tires of the main gear 1 is not exactly above the cables (Figure 6). The three parts of the landing gear of the A340-300 and the different spacing of the tires (central / main

gear) are clearly visible. The distance between the two main gears is 10.68 m (axis - axis (Figure 6). The measured strain distribution is not symmetric, which may be explained by the slightly misplaced location of the airplane in position a_3 (non-parallel rear gear axis to cable section 1) and potential inhomogeneity in the pavement. A reduction of strains was observed in the subsequent position a_4, where the center of the main gear is located approximately above section 1 of the sensor cable (but not the tires).

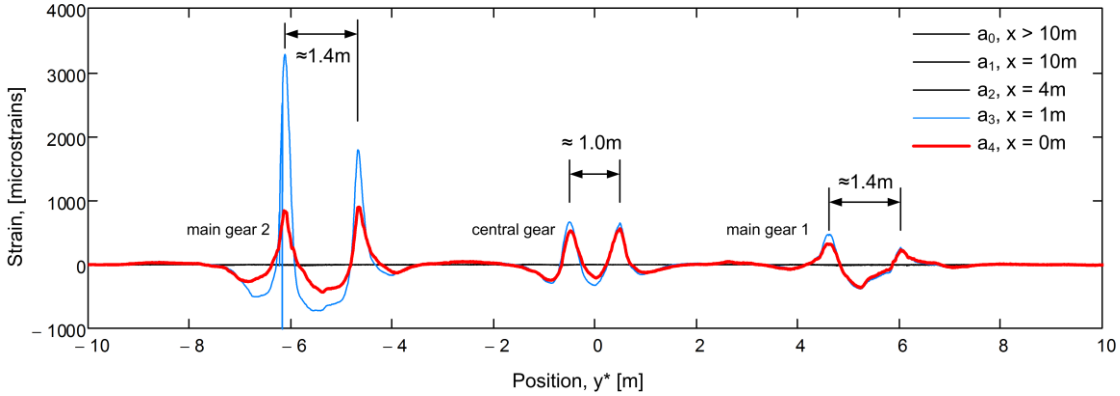

Figure 7: Strains measured along section 1 of BSST-V9 in 4 cm depth for different airplane positions

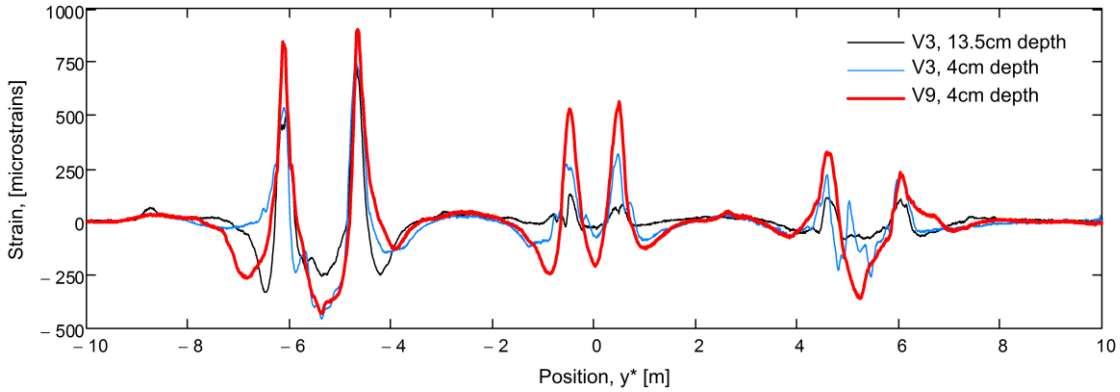

Figure 8: Strains measured along different sensors for airplane position a_4

Figure 8 shows the measured strain distribution for position a_4, where the center of the landing gear is located approximately above section 1 of the sensing cables, for all three installed strain sensors. This allows for a comparison of the strains measured in different depths and the performance of the different cables in the same depth. It can be observed that the BSST-V3 cable (Stiffer, consisting of more layers) seems to be slightly less capable to follow the high strain gradients in the pavement than the BSST-V9 cable. However, further investigation is required with respect to that. Furthermore, the strains just above the foundation layer in 13.5 cm depth are in general slightly smaller.

For the figures above, the positioning of the individual sensor responses were shifted relative to each other in order to match with the "footprint" of the airplane. Furthermore, the whole measured spectral shift between the reference measurement a_0 and the final measurement a_4 was converted at this preliminary stage to strain because the contribution of temperature to the spectral shift appeared to be negligible owing to the small temperature variation within the short test duration. This is also confirmed by the fact, that in the regions where no strain change is expected ($|y^*| > 9$ m), all lines in Figure 7 are close to zero. However, the fiber-optic sensor response under the high radial stress, when the gear tires are located directly above the cables, requires further investigation.

7 INVERSE ANALYSIS

The pavement strain field measured during aircraft loading (Figure 7 and 8) was adopted for carrying out a preliminary inverse analysis in order to estimate the mechanical properties of the pavement layers. A finite element (FE) model was developed adopting the commercial FE code ABAQUS. Taking advantage of the symmetries of the real problem, only ¼ of the landing gear was modelled. The model sizes (5 x 5 x 5.66 m = depth) were chosen in order to prevent the boundary conditions affecting the quality of the results. The layers were modelled with linear elastic constitutive models. The interaction between the layers is simulated with a frictional interface (friction coefficient = 0.5). The model has 86116 C3D8RH elements.

The tire and loading geometry are calculated according to AIRBUS specifications for empty aircraft and 7 tons of kerosene. The loading area was assumed rectangular area having sizes 0.30 m (length) x 0.36 m (width) with an inflating pressure of 14.2 bars.

The calculated strains are obtained in the model according to the real measured position of the aircraft against the cable (see also Figure 6).

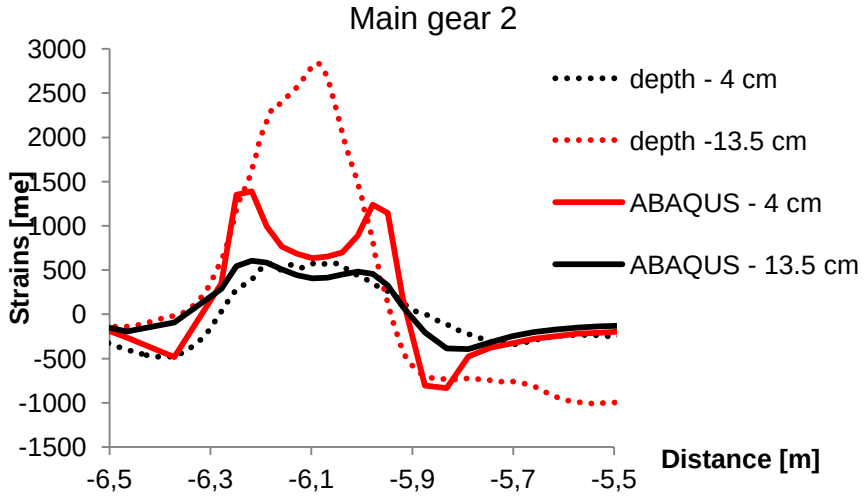

Figure 9: Measured and simulated strain at position a3 in 4 cm and 13.5 cm depth for main gear 2.

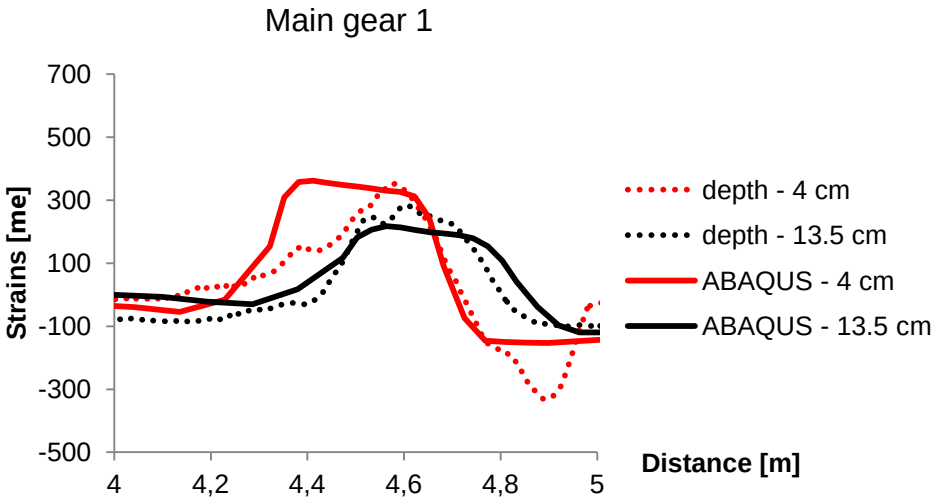

Figure 10: Measured and simulated strain at position a3 in 4 cm and 13.5 cm depth for main gear 1.

The preliminary results (Figure 9 and 10) show that the FE model reproduces reasonably well the strains measured at 4 and 13.5 cm depth with realistic layer stiffness values (Table 1). The back-calculated relatively low asphalt stiffness is due to the high temperatures and static load.

Table 1. Backcalculated layers stiffness

Material	E Modulus [MPa]	Poisson ratio [-]
AC 11 S	400	0.4
AC B 22 S	800	0.4
CTB (ZMO / ZMU)	3'000	0.17
Subgrade	45	0.3

The maximum strains in the top asphalt layers measured by the fiber optical sensor at the left landing gear could not be reproduced by the FE model. Instead of a peak, the FE model shows lower strain values in the middle of the tire. The likely reason of this discrepancy is a very simplified shape of the contact area and the homogenous loading pressure distribution adopted for this preliminary analysis. It is believed that the adoption of a more sophisticated constitutive model for asphalt (e.g. hyperelasticity, see also Rabaiotti 2009, Puzrin and Rabaiotti, 2010) could also allow achieving a better fitting of the experimental results.

8 DISCUSSION AND CONCLUSIONS

It could be shown that distributed fibre-optic sensors can be implemented directly into different layers of an asphalt pavement. The sensors particularly survived the harsh installation procedure during which the sensing cables are subjected to high temperatures and high loads induced by

the heavy compacting machine. Furthermore, the sensors were able to measure the strains induced by the rear landing gear of an airplane. The individual tires of the airplane could be clearly distinguished on the basis of the strain distribution along the sensing cable.

The inverse analysis shows that the measured strains can be reasonably reproduced by a relatively simple finite element model adopting linear elastic constitutive model for the layers. In order to achieve a better matching between measured and back-calculated strains a more realistic tire footprint shape and loading pressure distribution as well as more sophisticated constitutive models, in particular for asphalt, should be adopted.

Distributed fibre optic technology proved to be a remarkable sensing tool which could be of large potential benefit for the airport owners.

The results from the adopted technology could be very useful for detecting problem zones and quality issues in the realized pavement, as well as validating the assumptions made for the design. Potentially the installed sensors could also provide information on the development of the damage in the layers during the entire service life.

9 ACKNOWLEDGMENTS

The authors greatly acknowledge the support of Hanspeter Moll, Stephan Bruderer, Stefan Conrad and Thomas Hossli of the Flughafen Zürich AG and are grateful for the possibility to carry out this study on a real and important project for Zurich Airport.

REFERENCES

Arraigada, M., Partl, M.N., Angelone, S.M., Martinez. F. 2009. Evaluation of accelerometers to determine pavement deflections under traffic loads. *Materials and Structures.* Vol. 42, pp. 779 - 790.

Chapeleau, X., Blanc, J., Hornych, P., Gautier, J.L., Carroge, J. 2014. Use of distributed fiber optic sensors to detect damage in a pavement. *7th European Workshop on Structural Health Monitoring*, July 8-11, 2014. La Cité, Nantes, France

Froggatt, M. & Moore, J. 1998. High-spatial-resolution distributed strain measurement in optical fiber with Rayleigh scatter. *Applied Optics*, Vol. 37, No. 10, pp. 1735-1740.

Gifford, D.K., Kreger, S.T., Sang, A.K., Froggatt, M.E., Duncan, R.G., Wolfe, M.S. & Soller, B.J. 2007. Swept-wavelength interferometric interrogation of fiber Rayleigh scatter for distributed sensing applications. *Fiber Optic Sensors and Applications V*, Udd, E. (ed.), Proc. of SPIE, Vol. 6770, pp. 0F-1-0F-9

Horiguchi, T., Kurashima, T., & Tateda, M. 1989. Tensile strain dependence of Brillouin frequency shift in silica optical fibers. *IEEE Photonics Technology Letters*, Vol. 1, No. 5, pp. 107-108.

Kishida, K., Nishiguchi, K., Li, C.-H. & Guzik, A. 2009. An important milestone of distributed fiber optical sensing technology: separate temperature and strain in a single SM fiber. *14th OptoElectronics and Communications Conference (OECC).*

Mohamad, H. 2012. Temperature and strain sensing techniques using Brillouin optical time domain reflectometry. *Smart Sensor Phenomena, Technology, Networks and Systems Integration 2012*, Matikas, T.E., Peters, K.J. & Ecke, W. (eds.), Proc. of SPIE, Vol. 8346, pp. 1M-1 – 13

Niklès, M., Thévenaz, L. & Robert, P.A. 1997. Brillouin gain spectrum characterization in single-mode optical fibers. *Journal of Lightwave Technology*, Vol. 15, No. 10, pp. 1842-1851.

Niklès M. 2007 Fibre Optic distributed scattering sensing system: perspectives and challenges for high performance applications. *3rd European Workshop on Optical Fibre Sensors*, Proc. of SPIE vol. 6619, Naples, Italy, 2007, pp. D1-D8.

Puzrin, A.M., Rabaiotti, C. 2010. A thermomechanical framework for non-linear hyperviscoelastic materials. *Journal of Rheology*, Vol. 54, No. 3, pp. 619-642.

Rabaiotti, C. 2009. Inverse Analysis in Road Geotechnics. PHD Thesis no. 18135, ETH Zurich (Switzerland).

Wang, H., and Xiang, P. 2016. Strain transfer analysis of optical fiber based sensors embedded in an asphalt pavement structure. *Measurement Science and Technology*, Vol. 27, 075106.